HHS Public Access

Author manuscript

Mol Imaging Biol. Author manuscript; available in PMC 2018 January 24.

Published in final edited form as:

Mol Imaging Biol. 2017 October ; 19(5): 772–778. doi:10.1007/s11307-017-1052-3.

Source-based morphometry multivariate approach to analyze ^{123}I-FP-CIT SPECT imaging

E Premi[1,2], **VD Calhoun**[3], **V Garibotto**[4], **R Turrone**[1], **A Alberici**[1], **E Cottini**[1], **A Pilotto**[1], **S Gazzina**[1], **M Magoni**[2], **B Paghera**[5], **B Borroni**[1], and **A Padovani**[1]

[1]Neurology Unit, Department of Clinical and Experimental Sciences, University of Brescia, Italy [2]Stroke Unit, Azienda Ospedaliera "Spedali Civili", Spedali Civili Hospital, Brescia, Italy [3]The Mind Research Network and Lovelace Biomedical and Environmental Research Institute, Albuquerque, NM 87106, USA; Dept. of Psychiatry and Neurosciences, University of New Mexico, Albuquerque, NM 87131, USA; Dept. of Electronic and Computer Engineering, University of New Mexico, Albuquerque, NM 87131, USA [4]Department of Medical Imaging, Geneva university Hospital, Geneva, Switzerland [5]Nuclear Medicine Unit, Azienda Azienda ospedaliera "Spedali Civili", Spedali Civili Hospital, Brescia, Italy

Abstract

Background—^{123}I-FP-CIT (DaTSCAN®) SPECT imaging is widely used to study neurodegenerative parkinsonism, with the evaluation of presynaptic dopamine transporter (DAT) in striatal regions. Beyond DAT, ^{123}I-FP-CIT may be also considered for other monoaminergic systems, in particular serotonin transporter (SERT). Independent Component Analysis (ICA) implemented in Source-Based Morphometry (SBM), a multivariate approach, represents an alternative method to explore monoaminergic neurotransmission, studying the relationship among voxels, and grouping them into "metabolic" neural networks.

Methods—One-hundred forty-three subjects (84 with Parkinson's disease (PD) and 59 control individuals (CG)) underwent DATSCAN® imaging. The ^{123}I-FP-CIT binding was evaluated by the multivariate SBM approach, as well as by region-of-interest (ROI) (caudate/putamen) (BRASS software) and whole-brain voxelwise univariate (Statistical Parametric Mapping, SPM) approaches.

Results—As compared to univariate approaches (BRASS and SPM), which only demonstrated striatal ^{123}I-FP-CIT binding reduction in the PD group, SBM identified six sources of non-artifactual origin, including basal ganglia and cortical regions as well as brainstem. Among them, three sources (basal ganglia and cortical regions) presented loading scores (as index of ^{123}I-FP-CIT binding) significantly different between PD and CG. Notably, even though not significantly different between PD and CG, the remaining three non-artifactual sources were characterized by a predominant frontal, brainstem and occipito-temporal involvement.

Corresponding Author: Enrico Premi, MD, Neurology Unit, Department of Clinical and Experimental Sciences, University of Brescia, and Stroke Unit, Azienda Ospedaliera "Spedali Civili", "Spedali Civili" Hospital, Brescia, Italy, P.zale Spedali Civili, 1 - 25123 Brescia, Italy, Ph. +39-0303995632, Fax +39-0303995027, zedtower@gmail.com.

Financial disclosure related to research covered in this article: the authors report no conflict of interest.

Discussion—The concept of source blind separation by the application of ICA (as implemented in SBM) represents a feasible approach to be considered in ^{123}I-FP-CIT (DaTSCAN®) SPECT imaging. Taking advantage of this multivariate analysis, specific patterns of variance can be identified (involving either striatal or extrastriatal regions) that could be useful in differentiating neurodegenerative parkinsonisms.

Keywords

Parkinson's Disease; ^{123}I-FP-CIT imaging; Statistical Parametric Mapping; Source Based Morphometry

INTRODUCTION

In clinical practice, ^{123}I-FP-CIT (^{123}I-ioflupane, DaTSCAN®, GE Healthcare, Glattbrugg, Switzerland) SPECT imaging is widely used to study pre-synaptic dopaminergic changes [1, 2]. DaTSCAN® has been proved to be useful to differentiate between degenerative forms of parkinsonism, i.e. Parkinson's disease (PD), Progressive Supranuclear Palsy (PSP), Dementia with Lewy Body (DLB) and Multiple System Atrophy (MSA), from non-degenerative parkinsonisms, namely drug-induced parkinsonism (DIP), psychogenic parkinsonisms (PP), or essential tremor[3-6]. From a clinical point of view, image assessment has been focused on the evaluation of striatal regions, considering the high affinity of ^{123}I-FP-CIT for these regions [7, 8], as index of presynaptic dopamine transporter (DAT) impairment [9]. However, as previously suggested by studies in non-human primates [10], in healthy subjects [11] and in pharmacological studies [1, 12], ^{123}I-FP-CIT could be useful for the evaluation of other monoaminergic systems (i.e. serotonine transporter, SERT, norepinephrine transporter, NET) [13, 14], in extrastriatal regions (cortical and midbrain)[15-17].

Striatal ^{123}I-FP-CIT binding (primarily related to nigrostriatal neuronal integrity) can be evaluated by a number of different methods. A region-of-interest (ROI) approach is based on a semi-quantitative analysis of the striatal region compared to a reference (occipital) region, after normalizing all images to a standardized ^{123}I-FP-CIT template derived from healthy subjects (BRASS software, Brain Registration & Analysis Software Suite, Hermes Medical Solutions, Stockholm, Sweden) [18]. Furthermore, a whole-brain approach based on Statistical Parametric Mapping for SPECT ^{123}I-FP-CIT imaging has been proposed [19-21], with the possibility to perform voxelwise studies on different groups of subjects with different statistical paradigms, and with the possibility to explore extrastriatal regions[22-25].

Source blind separation through Independent Component Analysis (ICA) has been widely used in functional neuroimaging, in particular for functional Magnetic Resonance Imaging (fMRI) [26]. This statistical method efficiently separates multivariate signals into non-overlapping spatial and time components and is able to capture functional/metabolic brain areas that are "working together", thus representing functional brain neural networks [27]. In a data-driven fashion, ICA allows the removal of a great proportion of data noise, improving the signal-to-noise ratio [28]. More recently, ICA approach has been successfully applied to structural data (named Source Based Morphometry, SBM) [29, 30], relying on the assumption that functionally correlated brain regions show greater concordance on structural measures

as a result of mutually trophic influences or common experience-related plasticity [31, 32]. In contrast with the univariate approach of SPM (detecting the mean difference between two groups), SBM is based on a multivariate paradigm and considers the relationship among voxels, grouping them into “metabolic” neural networks. From this point of view, the SBM approach represents an interesting alternative method to explore monoaminergic neurotransmission by the application of ^{123}I-FP-CIT SPECT imaging. Taking advantage of the source blind separation of the variance in ^{123}I-FP-CIT by SBM, different sources could be identified, with potential clinical and neurobiological relevance. These considerations prompted the present study, aimed at evaluating multivariate (SBM) analysis application on ^{123}I-FP-CIT SPECT imaging in PD patients compared to a control group (CG) of patients with a clinical diagnosis of Essential Tremor (ET).

METHODS

Subjects

Consecutive patients with PD diagnosis according to UK Parkinson’s disease Society Brain Bank clinical criteria [33] and supported by at least one-year follow-up were recruited from the Neurology Unit, Department of Clinical and Experimental Sciences, University of Brescia, Italy. All individuals underwent routine laboratory analyses and brain structural Magnetic Resonance Imaging (MRI). A standardized neurological examination was carried out, including the Unified Parkinson Disease Rating Scale (UPDRS-III) and the Mini Mental State Examination (MMSE).

Patients with a history of alcohol or drug abuse were excluded from the study. As control group (CG), a series of patients with clinical diagnosis of Essential Tremor (ET) [34, 35] (all with a normal ^{123}I-FP-CIT imaging), were considered. Written informed consent from the subject was obtained for each procedure. The research protocol has been approved by the Ethics Committee of the Brescia Hospital, Brescia, Italy.

SPECT imaging

Intravenous administration of 110–185 MBq of ^{123}I-FP-CIT was performed 30 min after thyroid blockade (800 mg of KClO4) in all subjects. Taking into account that SERT blockers (like Selective Serotonine Reuptake Inhibitors, SSRI) may influence ^{123}I-FP-CIT binding ratios (especially for sertraline) leading to increases of striatal to occipital ratios of approximately 10%, antidepressant therapy, if present, was suspended three weeks before the assessment. Brain SPECT was performed using a dual-head gamma-camera (Infinia Hawkey, GE Healthcare Ltd) calibrated with 159 KeV photopeak and ±10% energy window. Rotational radius was minimized (<16 cm). 120 projections over 360° (40 s/view) were acquired using a step-and-shoot protocol at 3° intervals with the camera heads following a circular orbit (matrix size 128×128; zoom 1.1) resulting in 43 min of total scan time (Total counts 1.8-3 × 10^6). Data were reconstructed by filtered backprojection, with a Butterworth 3-dimensional (3D) post-filter (order = 10.0; cut-off 0.50 cycle/cm) and corrected for attenuation (Chang’s method, 0.12/cm^{-1}) [22]. Three different methods of analysis of ^{123}I-FP-CIT imaging were considered:

i. BRASS™ software (BRASS, Brain Registration & Analysis Software Suite, Hermes Medical Solutions, Stockholm, Sweden; http://www.hermesmedical.com/products/hybrid-nm-processing/brass.html) was used for region-of–interest (ROI) analysis of striatal regions. A single ROI over the occipital lobe was set as reference background uptake area, and specific ratios for each caudate/putamen were calculated. Between-groups (PD vs CG) differences were evaluated by univariate General Linear Model, considering age and gender as nuisance variables. Statistical threshold was set at $p<0.05$ [18, 22].

ii. Statistical Parametric Mapping (SPM8 Wellcome Department of Imaging Neuroscience; http://www.fil.ion.ucl.ac.uk/spm/); ^{123}I-FP-CIT template from 30 healthy controls [36] was used for normalization process. Individual ^{123}I-FP-CIT data were realigned, spatially normalized to ^{123}I-FP-CIT template in Montreal Neurological Institute space and smoothed (3D Gaussian filter with 8 mm Full Width at Half Maximum). Each voxel value of each scan was normalized to the mean value within the occipital cortex. An univariate General Linear Model, considering age and gender as nuisance variables was applied, with statistical threshold set at $p<0.05$ with a whole-brain false-discovery rate (FDR) correction for multiple comparisons [37].

iii. Source Based Morphometry (SBM): SBM was initially described to study co-varying patterns of alterations in structural Magnetic Resonance Imaging (MRI) (i.e. grey matter density [29], cortical thickness [38], fractional anisotropy [30]) in different conditions like healthy aging [39], schizophrenia [29, 40] and Parkinson's Disease [41]. In the case of structural data (i.e. MRI), SBM can be used to analyze images which have only a single image per subject (i.e. grey matter but also functional techniques like positron emission tomography (PET) or single-photon emission computed tomography (SPECT)). Preprocessed images used for SPM analysis (realigned, spatially normalized to ^{123}I-FP-CIT template in Montreal Neurological Institute space and smoothed) were considered for SBM analysis. Briefly, SBM used spatial independent component analysis (ICA) to decompose local ^{123}I-FP-CIT binding variation across subjects into sources of common variance, considering a subjects-by-voxels data matrix. ICA was calculated by GIFT toolbox (GroupICAT v4.0a; http://mialab.mrn.org/software/gift) [42], using a neural network algorithm (Infomax) that attempts to minimize the mutual information of the network outputs[43]; the number of sources was set to thirty, and to ensure reliability of the sources the decomposition was tested by using the ICASSO toolbox [44] by running Infomax 10 times with different initial conditions and bootstrapped data sets and selected the best (most central) run. Individual source maps were converted to Z-scores before entering group statistics, to obtain voxel values comparable across subjects. As previously described for SBM [29], the mixing matrix (containing the loading parameters for each subject and for each source) was used for statistical analysis, testing the difference between PD and CG groups, considering age and gender as nuisance variables. The statistical threshold was set at $p<0.05$ with whole-brain false-discovery rate (FDR) correction for multiple comparisons [37]. As previously described [29], source

matrix was used for visualization, scaling each map to unit standard deviation (SBM Z map) and threshold at |Z|>3.0. The maps of significant sources were then superimposed onto the MNI-normalized template brain.

Statistical analysis

Comparisons of demographic and clinical characteristics between groups (PD vs CG) were assessed via a Student's t-test for continuous variables and a χ^2 test for categorical variables; significance level was set at $p< 0.05$. The data were analyzed by IBM SPSS Statistics 22.0 for Windows.

RESULTS

Demographic and clinical characteristics of PD and CG were reported in Table 1. Age and gender were significantly different among PD and CG, and they were considered as nuisance variables in the analyses. BRASS analysis demonstrated significant ($p<0.001$) striatal (putamen and caudate) ^{123}I-FP-CIT binding reduction in PD compared to CG, as expected (Table 1). SPM analysis showed a single cluster (109880 voxels, $p<0.05$ FDR whole-brain) of bilateral basal ganglia reduction in PD (x,y,z: −26, −6, 2; T=17.23, left putamen; x,y,z: 26, −6, 4; T=14.57, right putamen; x,y,z: −16, 16, 0; T=9.35, left caudate; x,y,z: 14, 16, 2; T=9.20, right caudate), with no evidence of extrastriatal differences between groups (Figure 1).

For the SBM results, visual inspection of the 30 estimated sources highlighted obvious artifacts (i.e., signal near the external boundary of the brain or appearing primarily in grey matter-related regions) of 24 sources. Six sources of non-artifactual origin were then considered (see Figure 2) including basal ganglia and cortical regions (frontal, temporal and occipito-parietal) as well as brainstem (pons-midbrain). Among them, three sources presented loading scores (as index of ^{123}I-FP-CIT binding) significantly different between PD and CG (Table 2). In particular, source 8 and 23 included basal ganglia (putamen, caudate, thalamus) bilaterally, as well as cortical areas such as anterior cingulate, insula and frontal regions, whereas source 21 was characterized by a left-predominant involvement of basal ganglia/cortical areas. Notably, even if not significantly different between PD and CG, the remaining three non-artifactual involved frontal (source 10), brainstem (source 17) and occipito-temporal (source 18) regions.

DISCUSSION

In the present work, we explored the potential application of the multivariate approach of SBM to ^{123}I-FP-CIT SPECT imaging, taking advantage of the source blind separation procedure of ICA [26, 29]. After ICA estimation, six non-artifactual sources were identified. In particular, three sources (8, 21, and 23) were mainly characterized by basal ganglia areas in association with frontal and temporal regions. In line with the clinical indication for ^{123}I-FP-CIT SPECT imaging and previous literature data [1, 2], ^{123}I-FP-CIT binding was significantly impaired in PD patients in comparison to control group. Univariate approaches were able to detect only striatal ^{123}I-FP-CIT binding impairment in PD patients, however the SBM approach demonstrated significant involvement of cortical areas. Conversely, such cortical

(extrastriatal) involvement was not recognized by univariate approaches, even if the large cluster reported by SPM analysis partially included extrastriatal regions (but without peak activations).

Interestingly, the identification of three different sources centered on basal ganglia suggested that ^{123}I-FP-CIT biding might serve to answer to additional clinical questions. First of all, ^{123}I-FP-CIT imaging was able to explore molecular fronto-striatal connectivity, as previously reported [22, 23]. As already mentioned, voxels carrying similar information were grouped by ICA in sources that can be considered as "metabolic" pattern, reflecting a similar ^{123}I-FP-CIT binding in the different [29]. Beyond basal ganglia, sources (10, 17 and 18) identified by ICA were characterized by the involvement of cortical regions (10: frontal; 18: temporo-occipital) as well as brainstem (source 17). Considering the affinity of ^{123}I-FP-CIT for different neurotransmitters (DAT and SERT in particular) and literature data [3, 6, 25, 45-47], ^{123}I-FP-CIT binding in brainstem (pons) could be more related to SERT than to DAT neurotransmission. Nevertheless, taking into account that ICA maximized the statistical independence of the estimated sources, the variance of the signal (namely ^{123}I-FP-CIT) considered in one source (i.e. source 17) is highly "specific" for that spatial pattern. On the contrary, in all other types of analysis (ROI-based, SPM, spatial covariance analysis) ^{123}I-FP-CIT binding signal was considered "as a whole", including noise, white matter but also the influence of other brain regions. In other words, considering that in ^{123}I-FP-CIT imaging the highest signal-to-noise ratio was present in striatal regions, the evaluation of other brain regions could be hampered by striatal regions. In this sense, ICA approach implemented in SBM analysis, separating the multivariate signal of ^{123}I-FP-CIT binding in maximally independent sources, could be potentially able "to move the lens" from striatal to extrastriatal brain regions. Altogether, obtained sources from SBM analysis on ^{123}I-FP-CIT imaging (and in particular sources 10, 17 and 18) supported the idea that this approach could be very useful in differentiating Parkinson's Disease from atypical parkinsonisms [19, 46-51]. For instance, source 17, which maps brainstem, has the potential to be useful to PSP diagnosis. In addition, the evaluation of source 18, mapping occipital regions, has the potential to be helpful in DLB diagnosis.

Future studies considering atypical neurodegenerative parkinsonisms need to be performed to further evaluate the extra potential applications of ^{123}I-FP-CIT imaging as diagnostic tool in the spectrum of extrapyramidal syndromes.

Acknowledgments

We would like to thank all participants of the study and their families.

Study funding: the study was not supported by any financial organization.

References

1. Booij J, Tissingh G, Boer GJ, et al. [123I]FP-CIT SPECT shows a pronounced decline of striatal dopamine transporter labelling in early and advanced Parkinson's disease. Journal of neurology, neurosurgery, and psychiatry. 1997; 62(2):133–140.

2. Seibyl JP, Marek K, Sheff K, et al. Test/retest reproducibility of iodine-123-betaCIT SPECT brain measurement of dopamine transporters in Parkinson's patients. Journal of nuclear medicine : official publication, Society of Nuclear Medicine. 1997; 38(9):1453–1459.

3. Benamer TS, Patterson J, Grosset DG, et al. Accurate differentiation of parkinsonism and essential tremor using visual assessment of [123I]-FP-CIT SPECT imaging: the [123I]-FP-CIT study group. Movement disorders : official journal of the Movement Disorder Society. 2000; 15(3):503–510.

4. Lorberboym M, Treves TA, Melamed E, Lampl Y, Hellmann M, Djaldetti R. [123I]-FP/CIT SPECT imaging for distinguishing drug-induced parkinsonism from Parkinson's disease. Movement disorders : official journal of the Movement Disorder Society. 2006; 21(4):510–514. [PubMed: 16250023]

5. Brigo F, Matinella A, Erro R, Tinazzi M. [(1)(2)(3)I]FP-CIT SPECT (DaTSCAN) may be a useful tool to differentiate between Parkinson's disease and vascular or drug-induced parkinsonisms: a meta-analysis. European journal of neurology. 2014; 21(11):1369–e1390. [PubMed: 24779862]

6. Oh M, Kim JS, Kim JY, et al. Subregional patterns of preferential striatal dopamine transporter loss differ in Parkinson disease, progressive supranuclear palsy, and multiple-system atrophy. Journal of nuclear medicine : official publication, Society of Nuclear Medicine. 2012; 53(3):399–406.

7. Lundkvist C, Halldin C, Swahn CG, et al. [O-methyl-11C]beta-CIT-FP, a potential radioligand for quantitation of the dopamine transporter: preparation, autoradiography, metabolite studies, and positron emission tomography examinations. Nuclear medicine and biology. 1995; 22(7):905–913. [PubMed: 8547888]

8. Geisler S, Beindorff N, Cremer M, et al. Characterization of [123I]FP-CIT binding to the dopamine transporter in the striatum of tree shrews by quantitative in vitro autoradiography. Synapse (New York, NY). 2015; 69(10):497–504.

9. Catafau AM, Tolosa E. Impact of dopamine transporter SPECT using 123I-Ioflupane on diagnosis and management of patients with clinically uncertain Parkinsonian syndromes. Movement disorders : official journal of the Movement Disorder Society. 2004; 19(10):1175–1182. [PubMed: 15390019]

10. Laruelle M, Baldwin RM, Malison RT, et al. SPECT imaging of dopamine and serotonin transporters with [123I]beta-CIT: pharmacological characterization of brain uptake in nonhuman primates. Synapse (New York, NY). 1993; 13(4):295–309.

11. Kuikka JT, Tiihonen J, Bergstrom KA, et al. Imaging of serotonin and dopamine transporters in the living human brain. European journal of nuclear medicine. 1995; 22(4):346–350. [PubMed: 7607266]

12. Neumeyer JL, Tamagnan G, Wang S, et al. N-substituted analogs of 2 beta-carbomethoxy-3 beta-(4'-iodophenyl)tropane (beta-CIT) with selective affinity to dopamine or serotonin transporters in rat forebrain. Journal of medicinal chemistry. 1996; 39(2):543–548. [PubMed: 8558525]

13. Scheffel U, Lever JR, Abraham P, et al. N-substituted phenyltropanes as in vivo binding ligands for rapid imaging studies of the dopamine transporter. Synapse (New York, NY). 1997; 25(4):345–349.

14. Okada T, Fujita M, Shimada S, et al. Assessment of affinities of beta-CIT, beta-CIT-FE, and beta-CIT-FP for monoamine transporters permanently expressed in cell lines. Nuclear medicine and biology. 1998; 25(1):53–58. [PubMed: 9466362]

15. Gunther I, Hall H, Halldin C, Swahn CG, Farde L, Sedvall G. [125I] beta-CIT-FE and [125I] beta-CIT-FP are superior to [125I] beta-CIT for dopamine transporter visualization: autoradiographic evaluation in the human brain. Nuclear medicine and biology. 1997; 24(7):629–634. [PubMed: 9352533]

16. Kish SJ, Furukawa Y, Chang LJ, et al. Regional distribution of serotonin transporter protein in postmortem human brain: is the cerebellum a SERT-free brain region? Nuclear medicine and biology. 2005; 32(2):123–128. [PubMed: 15721757]

17. Isaias IU, Marotta G, Pezzoli G, et al. Enhanced catecholamine transporter binding in the locus coeruleus of patients with early Parkinson disease. BMC neurology. 2011; 11:88. [PubMed: 21777421]

18. Pencharz DR, Hanlon P, Chakravartty R, et al. Automated quantification with BRASS reduces equivocal reporting of DaTSCAN (123I-FP-CIT) SPECT studies. Nuclear medicine review Central & Eastern Europe. 2014; 17(2):65–69. [PubMed: 25088104]
19. Colloby SJ, O'Brien JT, Fenwick JD, et al. The application of statistical parametric mapping to 123I-FP-CIT SPECT in dementia with Lewy bodies, Alzheimer's disease and Parkinson's disease. NeuroImage. 2004; 23(3):956–966. [PubMed: 15528096]
20. Kaasinen V, Joutsa J, Noponen T, Johansson J, Seppanen M. Effects of aging and gender on striatal and extrastriatal [123I]FP-CIT binding in Parkinson's disease. Neurobiology of aging. 2015; 36(4):1757–1763. [PubMed: 25697414]
21. El Fakhri G, Habert MO, Maksud P, et al. Quantitative simultaneous (99m)Tc-ECD/123I-FP-CIT SPECT in Parkinson's disease and multiple system atrophy. European journal of nuclear medicine and molecular imaging. 2006; 33(1):87–92. [PubMed: 16180033]
22. Premi E, Pilotto A, Garibotto V, et al. Impulse control disorder in PD: A lateralized monoaminergic frontostriatal disconnection syndrome? Parkinsonism & related disorders. 2016
23. Frosini D, Unti E, Guidoccio F, et al. Mesolimbic dopaminergic dysfunction in Parkinson's disease depression: evidence from a 123I-FP-CIT SPECT investigation. Journal of neural transmission (Vienna, Austria : 1996). 2015; 122(8):1143–1147.
24. Eusebio A, Azulay JP, Ceccaldi M, Girard N, Mundler O, Guedj E. Voxel-based analysis of whole-brain effects of age and gender on dopamine transporter SPECT imaging in healthy subjects. European journal of nuclear medicine and molecular imaging. 2012; 39(11):1778–1783. [PubMed: 22890804]
25. Koch W, Unterrainer M, Xiong G, et al. Extrastriatal binding of [(1)(2)(3)I]FP-CIT in the thalamus and pons: gender and age dependencies assessed in a European multicentre database of healthy controls. European journal of nuclear medicine and molecular imaging. 2014; 41(10):1938–1946. [PubMed: 24806112]
26. Margulies DS, Bottger J, Long X, et al. Resting developments: a review of fMRI post-processing methodologies for spontaneous brain activity. Magma (New York, NY). 2010; 23(5–6):289–307.
27. Beckmann CF. Modelling with independent components. NeuroImage. 2012; 62(2):891–901. [PubMed: 22369997]
28. Zeman PM, Till BC, Livingston NJ, Tanaka JW, Driessen PF. Independent component analysis and clustering improve signal-to-noise ratio for statistical analysis of event-related potentials. Clinical neurophysiology : official journal of the International Federation of Clinical Neurophysiology. 2007; 118(12):2591–2604. [PubMed: 17967560]
29. Xu L, Groth KM, Pearlson G, Schretlen DJ, Calhoun VD. Source-based morphometry: the use of independent component analysis to identify gray matter differences with application to schizophrenia. Human brain mapping. 2009; 30(3):711–724. [PubMed: 18266214]
30. Caprihan A, Abbott C, Yamamoto J, et al. Source-based morphometry analysis of group differences in fractional anisotropy in schizophrenia. Brain connectivity. 2011; 1(2):133–145. [PubMed: 22180852]
31. Fornito A, Zalesky A, Breakspear M. The connectomics of brain disorders. Nature reviews Neuroscience. 2015; 16(3):159–172. [PubMed: 25697159]
32. Montembeault M, Joubert S, Doyon J, et al. The impact of aging on gray matter structural covariance networks. NeuroImage. 2012; 63(2):754–759. [PubMed: 22776455]
33. Hughes AJ, Daniel SE, Kilford L, Lees AJ. Accuracy of clinical diagnosis of idiopathic Parkinson's disease: a clinico-pathological study of 100 cases. Journal of neurology, neurosurgery, and psychiatry. 1992; 55(3):181–184.
34. Bain P, Brin M, Deuschl G, et al. Criteria for the diagnosis of essential tremor. Neurology. 2000; 54(11 Suppl 4):S7. [PubMed: 10854345]
35. Nicastro N, Garibotto V, Poncet A, Badoud S, Burkhard PR. Establishing On-Site Reference Values for (123)I-FP-CIT SPECT (DaTSCAN(R)) Using a Cohort of Individuals with Non-Degenerative Conditions. Molecular imaging and biology : MIB : the official publication of the Academy of Molecular Imaging. 2016; 18(2):302–312. [PubMed: 26341194]

36. Garcia-Gomez FJ, Garcia-Solis D, Luis-Simon FJ, et al. Elaboration of the SPM template for the standardization of SPECT images with 123I-Ioflupane. Revista espanola de medicina nuclear e imagen molecular. 2013; 32(6):350–356. [PubMed: 23570700]
37. Genovese CR, Lazar NA, Nichols T. Thresholding of statistical maps in functional neuroimaging using the false discovery rate. NeuroImage. 2002; 15(4):870–878. [PubMed: 11906227]
38. Steenwijk MD, Geurts JJ, Daams M, et al. Cortical atrophy patterns in multiple sclerosis are non-random and clinically relevant. Brain : a journal of neurology. 2016; 139(Pt 1):115–126. [PubMed: 26637488]
39. Eckert MA, Keren NI, Roberts DR, Calhoun VD, Harris KC. Age-related changes in processing speed: unique contributions of cerebellar and prefrontal cortex. Frontiers in human neuroscience. 2010; 4:10. [PubMed: 20300463]
40. Gupta CN, Calhoun VD, Rachakonda S, et al. Patterns of Gray Matter Abnormalities in Schizophrenia Based on an International Mega-analysis. Schizophrenia bulletin. 2015; 41(5): 1133–1142. [PubMed: 25548384]
41. Rektorova I, Biundo R, Marecek R, Weis L, Aarsland D, Antonini A. Grey matter changes in cognitively impaired Parkinson's disease patients. PloS one. 2014; 9(1):e85595. [PubMed: 24465612]
42. Calhoun VD, Adali T, Pearlson GD, Pekar JJ. A method for making group inferences from functional MRI data using independent component analysis. Human brain mapping. 2001; 14(3): 140–151. [PubMed: 11559959]
43. Bell AJ, Sejnowski TJ. An information-maximization approach to blind separation and blind deconvolution. Neural computation. 1995; 7(6):1129–1159. [PubMed: 7584893]
44. Himberg J, Hyvarinen A, Esposito F. Validating the independent components of neuroimaging time series via clustering and visualization. NeuroImage. 2004; 22(3):1214–1222. [PubMed: 15219593]
45. Ziebell M, Holm-Hansen S, Thomsen G, et al. Serotonin transporters in dopamine transporter imaging: a head-to-head comparison of dopamine transporter SPECT radioligands 123I-FP-CIT and 123I-PE2I. Journal of nuclear medicine : official publication, Society of Nuclear Medicine. 2010; 51(12):1885–1891.
46. Roselli F, Pisciotta NM, Pennelli M, et al. Midbrain SERT in degenerative parkinsonisms: a 123I-FP-CIT SPECT study. Movement disorders : official journal of the Movement Disorder Society. 2010; 25(12):1853–1859. [PubMed: 20669272]
47. Seppi K, Scherfler C, Donnemiller E, et al. Topography of dopamine transporter availability in progressive supranuclear palsy: a voxelwise [123I]beta-CIT SPECT analysis. Archives of neurology. 2006; 63(8):1154–1160. [PubMed: 16908744]
48. Davidsson A, Georgiopoulos C, Dizdar N, Granerus G, Zachrisson H. Comparison between visual assessment of dopaminergic degeneration pattern and semi-quantitative ratio calculations in patients with Parkinson's disease and Atypical Parkinsonian syndromes using DaTSCAN(R) SPECT. Annals of nuclear medicine. 2014; 28(9):851–859. [PubMed: 24997753]
49. Walker Z, Moreno E, Thomas A, et al. Clinical usefulness of dopamine transporter SPECT imaging with 123I-FP-CIT in patients with possible dementia with Lewy bodies: randomised study. The British journal of psychiatry : the journal of mental science. 2015; 206(2):145–152. [PubMed: 25431431]
50. Berding G, Brucke T, Odin P, et al. [[123I]beta-CIT SPECT imaging of dopamine and serotonin transporters in Parkinson's disease and multiple system atrophy. Nuklearmedizin Nuclear medicine. 2003; 42(1):31–38. [PubMed: 12601452]
51. Scherfler C, Seppi K, Donnemiller E, et al. Voxel-wise analysis of [123I]beta-CIT SPECT differentiates the Parkinson variant of multiple system atrophy from idiopathic Parkinson's disease. Brain : a journal of neurology. 2005; 128(Pt 7):1605–1612. [PubMed: 15817519]

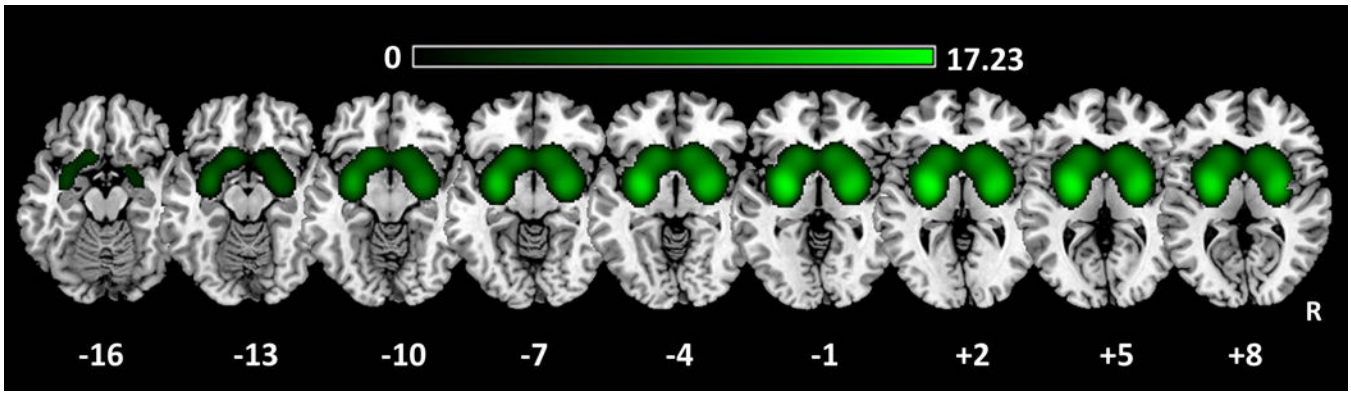

Figure 1. ^{123}I-FP-CIT (DaTscan®) imaging alterations in PD compared to CG with SPM approach

PD<CG contrast is presented (p<0.05 FDR whole-brain), showing the reduced DAT binding in basal ganglia bilaterally. Significant clusters were superimposed on a standardized MRI T1 3D template. Montreal Neurological Institute of standardized space are shown below of each slices. R: right. PD: Parkinson's Disease. CG: control group. SPM: Statistical Parametric Mapping.

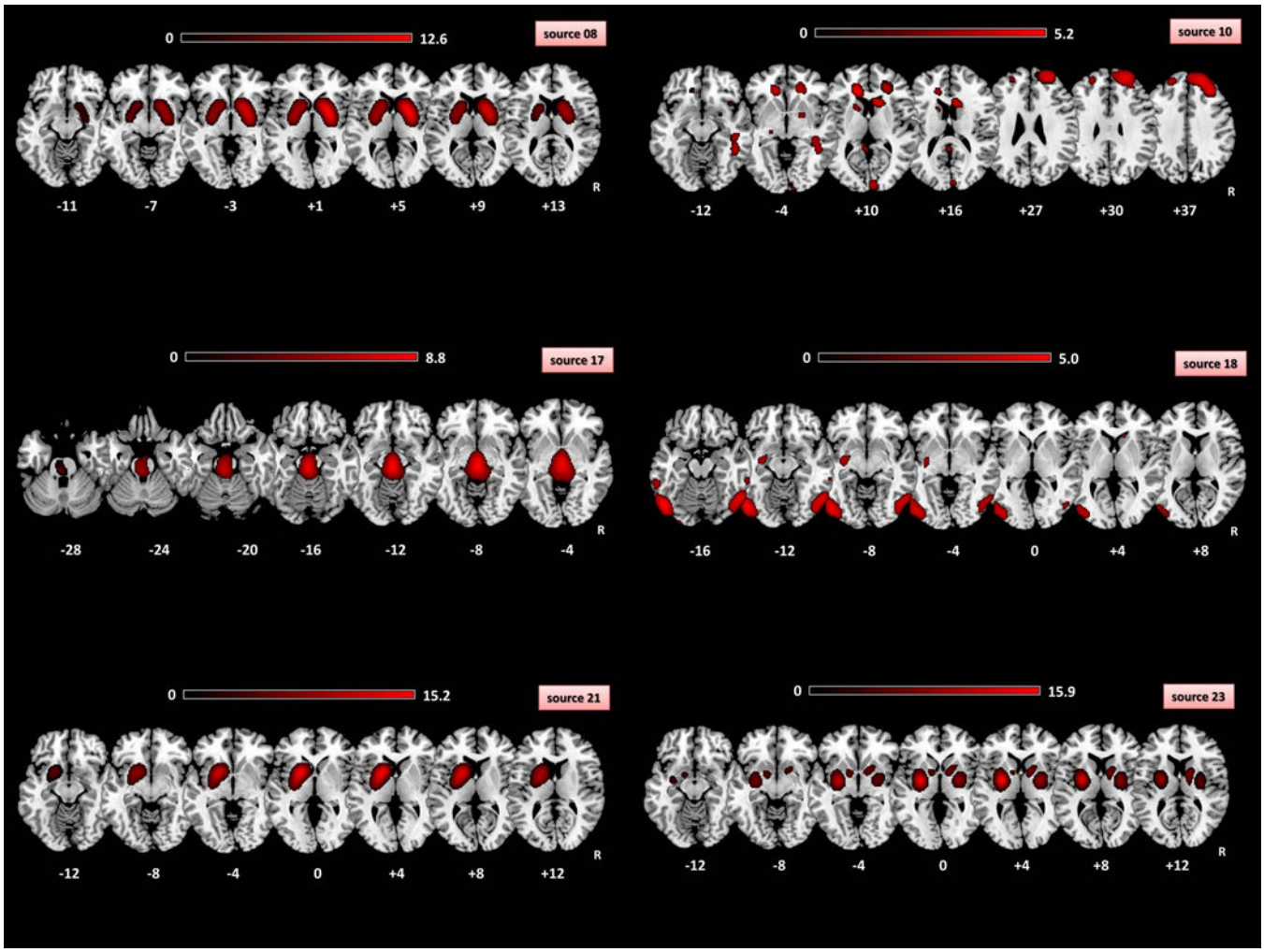

Figure 2. ^{123}I-FP-CIT (DaTscan®) imaging alterations in PD compared to CG with SBM approach

Each sources represented the absolute spatial pattern of the non-artifactual ^{123}I-FP-CIT binding derived from ICA analysis. Source 8: caudate and lentiform nuclei, insula anterior cingulate gyri; Source 10: bilateral inferior, middle, superior frontal gyri, right middle temporal and occipital gyri, caudate and lentiform nuclei, cingulate gyri; Source 17: pons, midbrain, bilateral posterior cingulate, thalami; Source 18: bilateral middle occipital, fusiform, inferior temporal, middle temporal, inferior occipital gyri; Source 21: left putamen, left caudate and left insula; Source 23: lentiform nuclei, caudate, insula, pons, right medial frontal gyrus and left inferior temporal gyrus. See Table 2 for details about the components significantly different between PD and CG. All the spatial components were thresholded at Z=3.0. Spatial patterns were superimposed on a standardized MRI T1 3D template. R: right. Montreal Neurological Institute of standardized space are shown below of each slices. R: right. PD: Parkinson's Disease. CG: control group. SBM: source-based morphometry.

Table 1

Demographic and clinical characteristics of the studied groups.

Variable	PD (n=84)	CG (n=59)	p
Age at evaluation, y	67.8±10.4	60.4±12.7	<0.001#
Gender, M % (n)	64.3% (54)	42.4% (25)	0.009^
MMSE	28.2±2.0	29.3±0.6	0.126#
UPDRS-III	15.1±7.5	-	-
L Caudate binding	1.58±0.44	2.61±0.43	<0.001°
R Caudate binding	1.69±0.50	2.79±0.42	<0.001°
L Putamen binding	1.14±0.51	2.71±0.40	<0.001°
R Putamen binding	1.10±0.52	2.62±0.45	<0.001°

Abbreviations and symbols: M, male; MMSE, Mini Mental State Examination; PD, Parkinson's Disease; CG, control group (DAT negative subjects); y, years; UPDRS-III, Unified Parkinson Disease motor score

t student test;

^ chi square test

° Univariate General Linear Model considering age and gender as nuisance variables. Caudate and Putamen bindings are expressed as ratio to occipital region of interest (ROI).

Table 2

Sources derived from SBM analysis significantly different among the studied groups (PD vs CG).

Component	Direction	Cluster	Region	MNI	mm^3
8	PD<CG	1	Putamen L	−24, 0, +2	8300
		2	Putamen R	+22, +4, +2	9400
		3	Caudate L	−12, +14, +2	2400
		4	Caudate R	+12, +12, +2	3700
		5	Insula L	−36, 0, +2	200
		6	Insula R	+36, 0, 0	500
		7	Thalamus R	+14, −6, +6	400
		8	Anterior Cingulate L	−12,+22, −4	100
		9	Anterior Cingulate R	+12, +22, −6	300
21	PD<CG	1	Putamen L	−20, +8, +2	8100
		2	Caudate L	−14, +16, +2	3600
		3	Insula L	−36, −8, +8	1300
23	PD<CG	1	Putamen L	−28, −6, +2	4700
		2	Putamen R	+26, −6, +4	3800
		3	Insula L	−36, −2, +2	1300
		4	Insula R	+36, −2, −2	200
		5	Pons L	−16, −14, −18	200
	PD>CG	1	Pallidum L	−12, +2, −4	600
		2	Pallidum R	+14, +6, 0	1900
		3	Thalamus L	−12, −10, +16	1000
		4	Thalamus R	+14, −8, +14	800
		5	Caudate L	−8, +4, 0	300
		6	Caudate R	+12, −2, +18	1300
		7	Medial Frontal gyrus R	+8, +26, −20	300
		8	Inferior Temporal gyrus L	−40, −12, −34	100

PD: Parkinson's Disease; CG: control group; MNI: Montreal Neurological Institute coordinates system; L: left; R: right; mm^3: cluster dimension expressed in cubic millimeter.